·Article·
Advances in Polar Science
doi: 10.3724/SP.J.1085.2013.00050
March 2013 Vol. 24 No. 1: 50-59

Assessing Doppler velocities of Rankin Inlet *F*-region echoes

Alexander V Koustov[1*], Kale Colville[1], Robyn A D Fiori[2] & Mohsen Ghezelbash[1]

[1] University of Saskatchewan, Saskatoon S7N 5E2, Canada;
[2] Geomagnetic Laboratory of Natural Resources Canada (NRCan), Ottawa K1A 0Y3, Canada

Received 29 August 2012; accepted 7 January 2013

Abstract Doppler velocities observed by the Rankin Inlet (RKN) PolarDARN radar are assessed with a focus on data in the beams oriented roughly along the magnetic meridian. Hourly scatter plots for every month are built. They are shown to vary widely, with median values showing very clear magnetic local time variation with maximum magnitude during pre-noon and pre-midnight hours. The histograms contain a significant amount of very small velocity data that dominates at farther ranges and during the daytime. Near noon data show generally antisunward flows but at large ranges/magnetic latitudes and very close to noon, sunward flows occur for periods of positive IMF B_z. The reverse flows are stronger during spring equinox. The velocity magnitude was found to depend linearly on the IMF B_z and interplanetary electric field. Velocities are often found to be smaller than those expected from the statistical convection model of Ruohoniemi and Greenwald –1996.

Keywords **PolarDARN radars, Doppler velocity, seasonal and magnetic local time variations**

Citation: Koustov A V, Colville K, Fiori R A D, et al. Assessing Doppler velocities of Rankin Inlet *F*-region echoes. Adv Polar Sci, 2013, 24:50-59, doi: 10.3724/SP.J.1085.2013.00050

1 Introduction

One of the major products of the Super Dual Auroral Radar Network (SuperDARN) project are global-scale ionospheric plasma circulation maps. These are inferred from Doppler velocity measurements from individual radars under the assumption that the velocity measured is the cosine component of the $\boldsymbol{E}\times\boldsymbol{B}$ plasma drift. Routinely, the velocity data from individual radars are not investigated; they are automatically added to a common data block. However, it is interesting to examine characteristics of the velocity measured by individual radars of the network, specifically, their diurnal, seasonal and solar cycle trends. In this respect, of special interest are observations during the last several years for which the plasma circulation maps are dominated by measurements with the two PolarDARN radars located at Rankin Inlet (RKN) and Inuvik (INV).

The PolarDARN velocities are of interest for several reasons. First, SuperDARN velocity measurements of plasma flow through the central polar cap are very limited. This is because with typical auroral zone SuperDARN radars the echoes at these latitudes can mostly be detected via one and half hops propagation mode. This requires specific ionospheric conditions, to bend the radar wave, and these conditions are not always easy to satisfy. It is not a surprise that SuperDARN plots are typically limited to magnetic latitudes equatorward of 80°, see for example Figure 2 of Ruohoniemi and Greenwald[1]. The PolarDARN radars detect echoes in the polar cap via the direct propagation mode, and they significantly outperform the auroral zone radars in terms of echo occurrence[2].

Secondly, the polar cap plasma flows are expected to saturate for extreme values of external drivers of the global plasma circulation, often characterized by the Interplanetary Magnetic Field (IMF) and Interplanetary Electric Field (IEF). Fiori et al.[3] attempted to look at this effect by comparing RKN velocities with the Polar Cap North (PCN) magnetic index, but the amount of data significantly dropped off as magnetic activity increased (PCN>4). It would be interesting to investigate the effect further.

* Corresponding author (email: sasha.koustov@usask.ca)

The HF echo occurrence at high latitudes is more frequent during equinoxes[4]. It would be interesting to see if this is coupled with enhanced $\boldsymbol{E}\times\boldsymbol{B}$ drifts during these seasons. One would expect such relationship because the gradient-drift plasma instability, the major source of *F*-region ionospheric irregularities, depends on the electric field[5]. Eventually, the solar cycle effect in Doppler velocity would be interesting to investigate, but up until now PolarDARN data are only available for years during solar minimum.

Finally, there is a general feeling that some RKN velocities could be a mixture of ionospheric and ground scatter so that the observed velocities do often not reflect $\boldsymbol{E}\times\boldsymbol{B}$ plasma drifts. This effect has been discussed by Chisham and Pinnock[6] with respect to other SuperDARN radars. Direct comparison of the RKN and INV velocities with $\boldsymbol{E}\times\boldsymbol{B}$ measurements from the Canadian Digital Ionosondes (CADI) and the Defense Meteorological Satellite Program (DMSP) satellites showed occasional significant discrepancies between the instruments[7-8]. These can be related to non $\boldsymbol{E}\times\boldsymbol{B}$ flows as observed by the SuperDARN radars.

The goal of this study is a general assessment of the RKN velocity, investigation of the velocity relationship with external drivers and comparison of the velocities with a statistical model of the high-latitude plasma circulation.

2 Rankin Inlet radar field of view and data selection

In this study we concentrate on RKN observations. Data for the INV radar are consistent with those reported for the RKN radar. Figure 1 shows the location of Rankin Inlet and Inuvik PolarDARN radars and their fields of view (FoVs) for range gates 5−50. The range in kilometers to the target gate can be calculated from the equation: *range*=180+*gate*×45, km. In the present work, we focus on measurements in beams 6, 7 and 8; these are shown in Figure 1 by grey shading. These beams were selected because they are roughly aligned in the direction of the magnetic meridian so that the velocities reflect the meridional component of the plasma flow which is of special importance for observations near magnetic noon and midnight when the $\boldsymbol{E}\times\boldsymbol{B}$ flows are predominantly meridional. We also consider a limited number of range gates, between 9 and 45. At shorter ranges, *E*-region echoes are usually detected. Since their velocities do not always reflect the $\boldsymbol{E}\times\boldsymbol{B}$ flows, they are not of interest to this study. Measurements at farther ranges are not considered here because the amount of RKN data is not significant there[2-3]. The dark rectangular area in Figure 1 denotes radar beams and gates for which more detailed analysis was performed and to which numerous references will be made.

3 Data presentation

Data for the year 2010 were selected as a major period for this study. Data for other years of RKN operation (2007−2011) show similar tendencies.

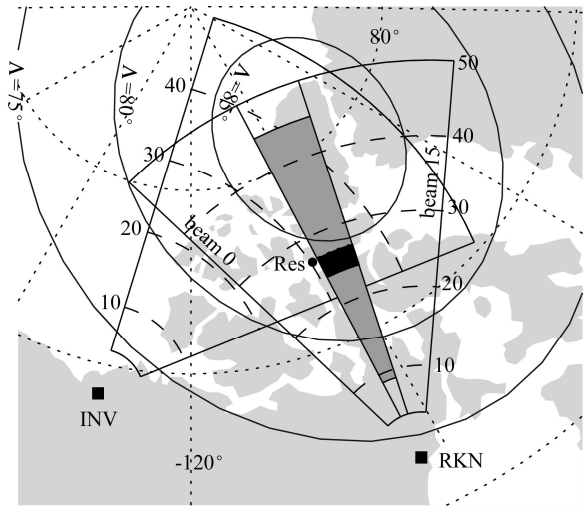

Figure 1 Locations and fields of view of the Rankin Inlet (RKN) and Inuvik (INV) HF radars. The dot indicates the location of Resolute Bay. The light shading shows the beam/gates of the radar data used in this study as described in the text. The black rectangle is the area within which data were largely discussed in the text. Heavy lines represent geomagnetic latitudes of 60°, 70° and 80°.

3.1 Daily variation of the velocity

Figure 2a presents all velocities measured by the RKN radar in March 2010 in range gates 24−26. More than 52 000 points are available. The reason for the selection of March data (i.e. for the equinox) is that echoes are observed frequently during all hours of the day, as opposite to other seasons when echoes occur predominantly during near magnetic noon hours (12 MLT).

The magnetic noon (midnight) for the RKN radar location is around 1830 (0630) UT. Visually, more echoes were detected during dusk-midnight-dawn hours. In this period, the cloud of points shows a general shift to larger positive velocities with maximum values achieved around midnight. The trend for the data in the dawn-noon-dusk sector is confusing. The velocities become more and more negative after 1000−1200 UT but around noon the positive velocities seem to occur as frequent as the negative velocities. Later, after ~2200 UT, the velocities are predominantly negative. To show the differences between near noon and midnight observations more explicitly, we show distributions of the velocity in these two sectors, in Figures 2c and 2d. Figure 2c (midnight) shows bell-shaped distribution with a maximum around 250 $m\cdot s^{-1}$. This distribution is fairly wide, ~1000 $m\cdot s^{-1}$, but consistent with observations of the auroral zone radars at lower latitudes, e.g. references 9 and 10. Figure 2d (noon) shows about equal occurrence of echoes with positive and negative velocity. We note that the distribution has a minor peak at 500 $m\cdot s^{-1}$. This peak is reminiscent of observations with the Hankasalmi radar[11] although its peak at 500 $m\cdot s^{-1}$ was very pronounced. The positive near-noon velocities are unexpected if the plasma circulation pattern is two-cell like. The initial hypothesis for

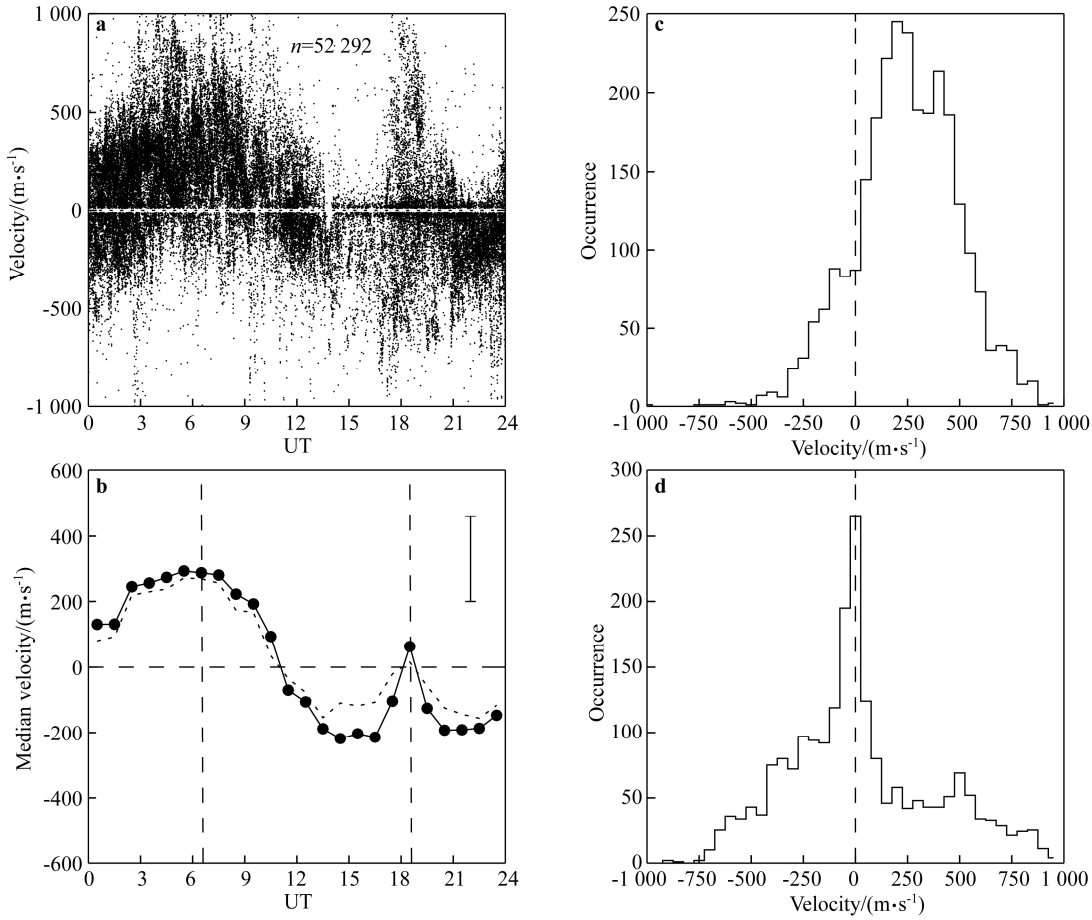

Figure 2 Scatter plot of the RKN velocity versus UT time observed in March 2010. Measurements in beams 6, 7 and 8 and range gates 24, 25 and 26 were considered (**a**). Total number of available points (*n*) is indicated. **b**, Median values of the RKN velocity for 1-hour UT time bins. Dotted line corresponds to medians for all velocities available in each bin while black dots connected by solid line correspond to medians for velocities with the magnitudes above 50 m·s^{-1}. Vertical bar represents a typical standard deviation of the velocity in various bins. Vertical dashed lines indicate approximate time for the magnetic midnight (0630 UT) and magnetic noon (1830 UT). For the beams considered, the magnetic local time is close to the local solar time. **c**, Histogram distribution of the measured velocities between 0600−0700 UT for the data presented in panel **a**. **d**, The same as **c** but for measurements between 1800 and 1900 UT.

the occurrence of the positive near noon velocities was the onset of sunward (reverse) plasma flows during intervals with positive B_z. This hypothesis will be pursued later.

The other feature recognizable in Figure 2a is the frequent occurrence of low-velocity data with velocity magnitudes of <50−100 m·s^{-1}. These are seen as horizontal "stripes" around the zero velocity line between ~1600 and 2400 UT. Domination of the low-velocity data with velocity magnitudes below 100 m·s^{-1} is obvious in Figure 2d.

To infer velocity trends in a quantitative way, we binned the data with 1-hour periods and selected the median value for each bin, Figure 2b. Two kinds of medians were used here, one for all data in a bin (shown by dotted line in Figure 2b) and another for all velocities with magnitudes above 50 m·s^{-1} in a bin (shown by solid line with large dots in Figure 2b). In Figure 2b the trends are similar for both types of binned velocities with the first type showing smaller magnitudes. The differences are more significant in the dawn-noon-dusk sector where low-velocity data constituted a significant portion of all points. Both types of medians show maximum values of ~300 m·s^{-1} near midnight and small positive values around noon. In the following analysis, data with velocity magnitude below 50 m·s^{-1} will not be considered. The reason for this is that these data may affect the median velocity values in significant way, as evidenced by the data in Figure 2b. The reason for low-velocity echo occurrence is not clear. One hypothesis is that these are mixed ground-scatter/ionospheric echoes or misidentified ground scatter echoes. These hypotheses require further investigation.

3.2 Low-velocity echoes

Although the low-velocity data were excluded from the statistical assessment of typical RKN velocities, we attempted to infer the typical pattern in their occurrence. We consider in this section echoes with the velocity magnitude

below 50 m·s^{-1}, echo power above 3 dB and spectral width below 500 m·s^{-1}. Figures 3a and 3b show UT variations of the proportion of low-velocity echoes to all echoes detected for winter (December 2010) and equinox (March 2010), respectively. Data for the summer period shows a predominant occurrence of low-velocity echoes most of the time with less frequent occurrence during near noon periods, but the amount of data is not as significant as for other seasons, and so they are not presented.

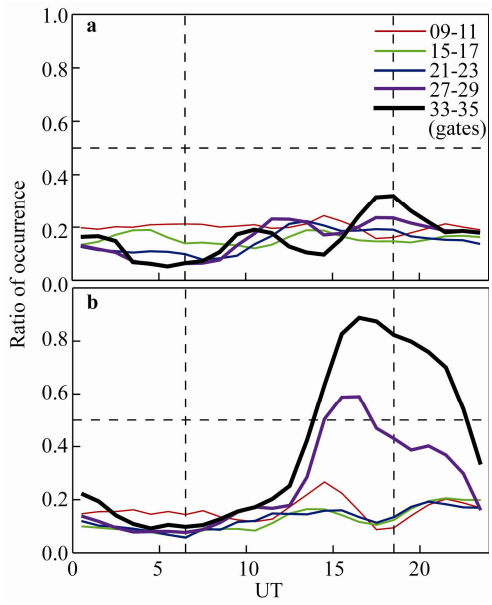

Figure 3 UT variation of the hourly ratio of the number of low velocity data (magnitude <50 m·s^{-1}) to the number of all data in each 1-hour bin for Decemebr 2010 (**a**) and March 2010 (**b**). Data in RKN beams 6, 7 and 8 and various range gates were considered; every group of range gates is represented by a line of certain thickness. The legend for the line thickness is shown in the top right corner of panel (**a**).

Figure 3a shows that the proportion of low-velocity echoes varies between 0.1 and 0.3 with the largest values near magnetic (and local solar) noon and in largest range gates of 21−35. In smaller range gates of 9−17, the variability is not as strong. In gates 21−35, another enhancement is seen around 1000−1400 UT. This enhancement is expected as during this period the radar beams are oriented perpendicular to the average flow. The data of Figure 3a support the notion that the daytime RKN echoes during winter can be related to the ground scatter that is strongest during these hours[12]. The preferential occurrence of low-velocity echoes at near noon hours is more obvious for observations in March 2010 at range gates 27−35, Figure 3b. For range gates 9−23, there is no such effect. Although the data presented show typical situations, data for some individual months show somewhat different patterns in occurrence implying that a more thorough investigation is required. Such a study might explain the reasons for the occurrence of low-velocity echoes.

3.3 Typical velocities at various ranges and radar look directions

To assess the velocity of RKN *F*-region echoes we plot hourly median velocity values for various radar look directions, ranges and UT time, Figure 4. All four plots in Figure 4 have the same x and y axis; UT time and radar range gate, respectively. The contour color scheme is the same in all plots. The plots go from the west-oriented beams 0−2 (Figure 4a), to central beams 6−8 (Figure 4b) and 9−11 (Figure 4c) to the east-oriented beams 13−15 (Figure 4d).

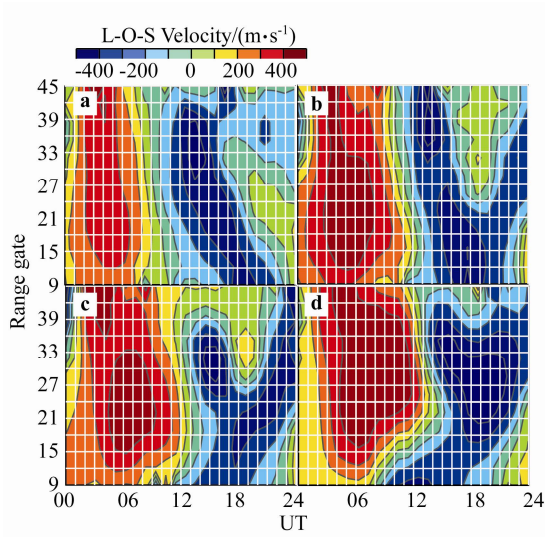

Figure 4 Contour plot of the RKN velocity (hourly medians) versus UT time at various radar ranges for observations in beams as follows: **a**, 0−2; **b**, 6−8; **c**, 9−11; **d**, 13−15. Data for March 2010 were considered. Contours are 100 m·s^{-1} apart.

There is a great deal of similarity between the plots. All show positive velocities between ~0000 and ~ 1200 UT, i.e. for observations on the nightside. During these hours, the largest velocities are observed close to the local midnight (0630 UT) in most east-oriented beams (13−15) with magnitudes in excess of 400 m·s^{-1}. Between ~0800 UT (Figure 4a) and ~1300 UT (Figure 4d), the polarity of the velocity changes to negative. The largest magnitudes of negative velocities are observed again in most east-oriented beams (13−15) close to the local noon (1830 UT). The maximum values here are in access of 400 m·s^{-1}. These values are also achieved in the most west-oriented beams (0−2) but in very limited range gates and a limited time sector. Earlier “transition” from positive to negative velocities for west-oriented beams as compared to east-oriented beams is expected if the plasma circulation pattern is predominantly two-celled.

At near noon hours, the plots for the central beams (6−8 and 9−11) are quite different from the ones at two other beam orientations as one can clearly see the occurrence of positive velocities indicated by contours with green color. The effect is stronger in beams 9−11. Such

velocities are not seen at range gates smaller than ~24.

3.4 Seasonal variations of the velocity at latitudes of Resolute Bay

To show the seasonal variations in the velocity of RKN echoes we plot hourly-medians in gates 24−26 of beams 6−8 (meridionally oriented beams) for all 5 years of continuous operation, Figure 5. The plot clearly shows (1) a transition from negative to positive velocities between 1000 and 1200 UT, (2) maximum velocity magnitudes near midnight and noon, and (3) the occurrence of "islands" of echoes with velocities of positive polarity. Interestingly enough, the near-noon positive velocities occur predominantly during spring equinox. A similar plot for range gates 27−29 also shows the occurrence of such flows during spring equinox. Importantly, such plots do not show this effect at smaller range gates. Another interesting feature of Figure 5 data is that maximum magnitudes of negative velocities are observed during summer season. This feature is not repetitive on plots for other range gates, and is likely an anomaly.

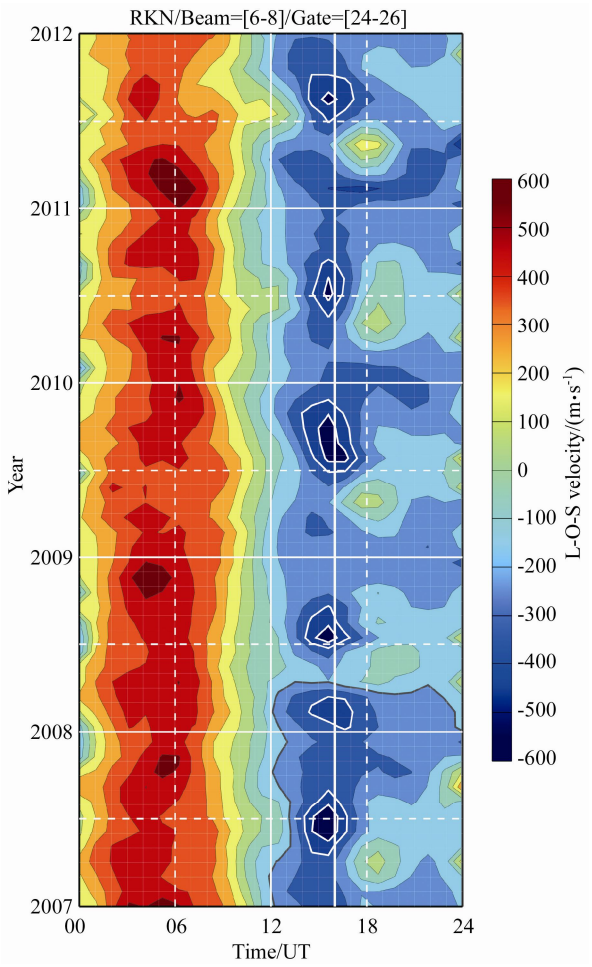

Figure 5 Variation of the RKN velocity (hourly medians) with UT time in beams 6, 7 and 8 and at radar range gates 24, 25 and 26 for observations in 2007−2011. Contours are 100 m·s^{-1} apart.

3.5 Positive near noon velocities and IMF B_z polarity

To test whether the near-noon positive velocities occur under positive B_z conditions, and are thus due to the onset of sunward (reverse) flows, we made histogram distributions of the velocity in beams 6−8, range gates 24−26 for observations under IMF B_z positive (B_z^+) and IMF B_z negative (B_z^-) conditions, Figure 6. For completeness, histograms are presented for midnight observations as well. According to Figure 6a, there are very few positive velocities for B_z^- conditions while they are abundant for B_z^+ conditions, Figure 6b. Contrary to this, velocities are almost all positive for the midnight observations irrespective of the B_z polarity.

3.6 Velocity in meridional beams and external drivers, IMF B_z and IEF

Since the RKN beams 6−8 are oriented roughly along the magnetic meridian, one would expect a velocity magnitude dependence on the IMF B_z and the IEF, as these are the major drivers of the high-latitude plasma circulation. Figure 7 shows scatter plots of the RKN velocity in gates 24–26 as a function of (a) IMF B_z and (b) IEF for near noon observations. Figures 7c and 7d are similar plots but for midnight observations. For the data presented in Figure 7 only periods with $|B_z|>|B_y|$ were considered to avoid possible involvement of the IMF B_y component in the formation of a plasma circulation pattern. The IEF was computed as a product of solar wind velocity and IMF B_z. Data on the IMF and solar wind were taken from the OMNI data base with an addition 8-min shift to allow disturbance propagation from the bow shock to the ionosphere.

The raw data in Figures 7a and 7b are spread along the bisectors in the quadrants 1 and 3. To characterize the dependence, the raw data were binned (1-nT steps for Figure 7a and 0.5-mV·m^{-1} steps for Figure 7b), and the linear fit lines were computed for the binned values of the velocity (red solid dots). The slopes of the lines a and the y-intercepts b are reported on each of the panels. Both a and b values vary from one month to another, however, the reported numbers for the slope are very typical, 70−100 m·s^{-1}·nT^{-1} and 150−200 m^2·s^{-1}·(mV)$^{-1}$ for the dependence upon B_z and IEF, respectively. The slopes for the nighttime dependences are usually smaller.

As expected, the midnight observations, Figures 7c and 7d do not show much anti-sunward flows (the velocities are mostly positive). The slopes of the best fit lines (calculated for the binned values of the velocity, similarly to Figures 7a and 7b) are smaller than the ones for the near noon observations indicating a weaker response of the plasma flows on the external drivers on the nightside. Comparing the nighttime data for positive and negative IMF B_z, Figure 7c, one can conclude that the slopes of the lines are comparable. Plots for the velocity versus IEF, Figure 7d, show stronger dependence for positive IEFs. This is perhaps not a real effect as the data for positive IEFs are

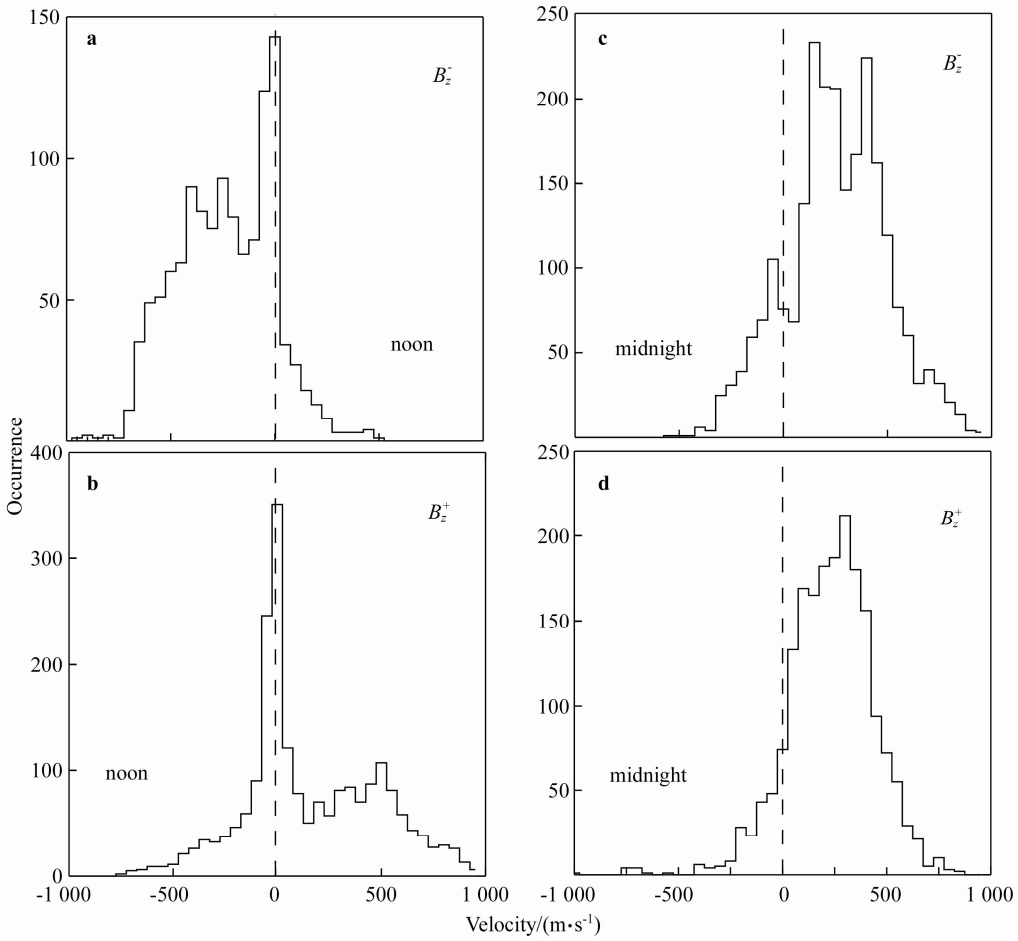

Figure 6 Histogram distribution of the RKN velocity for the echoes observed in March 2010 under **a**, **b** IMF B_z^- conditions and **c**, **d**, IMF B_z^+ conditions. **a** and **b** are for the noon sector (18−19 UT) while **c** and **d** are for the midnight sector (06−07 UT).

scarce at large IEFs.

3.7 Comparison with the Ruohoniemi-Greenwald −1996 model

Velocity measurements of the PolarDARN radars have not been used yet in the development of the statistical models of the high-latitude plasma circulation, including the most recent model by Pettigrew et al.[13]. The PolarDARN data, however, would be beneficial to use as it would improve the quality of the model predictions at polar cap latitudes. We note that the polar cap data ingested into the existing models were limited. In addition, as was mentioned earlier, the velocity of some echoes could be non $\boldsymbol{E}\times\boldsymbol{B}$-related and consideration of such data might introduce errors in the model. Investigation of the consistency between the statistical model predictions and the actual RKN measurements in the polar cap thus has a merit.

To date, SuperDARN convection maps have been predominantly produced (with results published) using the Ruohoniemi and Greenwald−1996[1] model (we will be referring to it as the RG-96 model). To be consistent with published research, the RG-96 model will be used in this paper. The RG-96 model is based on long-term data from the Goose Bay radar located in the auroral zone. In this section we investigate the consistency between the RG-96 model predictions and the actual RKN measurements in the polar cap. We select for presentation one specific latitude, MLAT=83°, the latitude of Resolute Bay, Figure 1.

The RG-96 model is parameterized by the IMF transverse component $B_t = \sqrt{B_z^2+B_y^2}$ and the IMF clock angle. Possible clock angles are grouped into eight 45° sectors centered at clock angles θ of 0°, 45°, 90° and so on. All possible combination of the RG-96 model parameters were considered, but only the results for $0 \leqslant B_t \leqslant 4nT$ and various clock angles for this range of B_t are presented, as the amount of data was the largest for this range of B_t. Also, results were limited to winter conditions and, to have reasonable statistics, data for December of 2007, 2008, 2009 and 2010 were combined into one block. In addition, the clock angle sectors were enlarged to 90°. To make comparison with the RKN measurements in the meridional beams straightforward, the northward component of the total RG-96 velocity vector was considered.

Figure 8 presents results of the comparison for four different sectors of the IMF clock angle as shown in each panel. Each cross in Figure 8 represents the median value of the velocity during the respective hour. In computing the

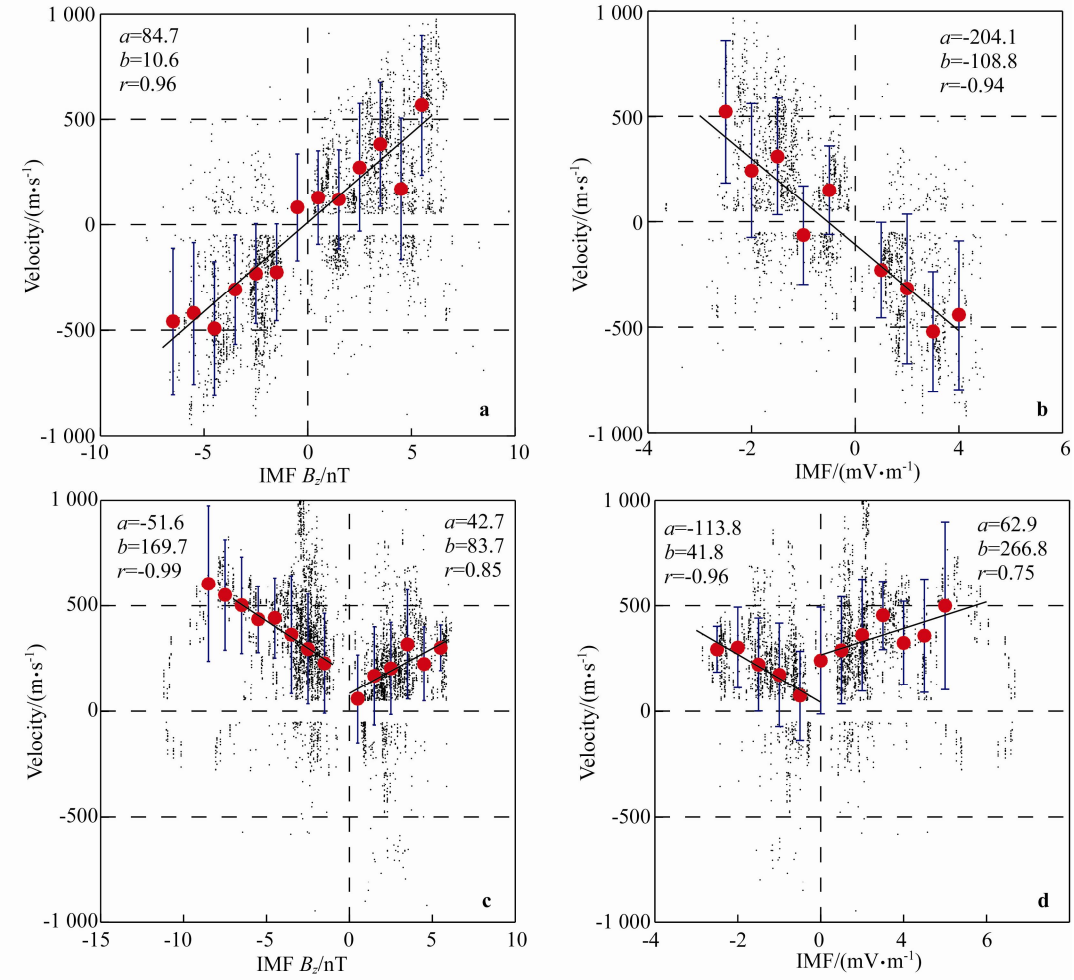

Figure 7 Scatter plots of the RKN velocity versus **a**, **c** IMF B_z and **b**, **d** interplanetary electric field (IEF) for observations at near magnetic noon hours (panels **a** and **b**, 1800−1900 UT) and at near midnight hours (panels **c** and **d**, 0600−0700 UT). Observations with $|B_z|>|B_y|$ were only considered. All the data were collected in RKN beams 6−8 and range gates 24−26.

median values, all velocity values available for a specific hour were considered, including low-velocities with magnitudes below 50 m·s^{-1}. This has been done as no filtering of the raw data has been done in data selection for the RG-96 model. The vertical bar by each cross in Figure 8 denote the standard deviation from the median value for each bin. These bars can be treated as the typical spread of the velocities observed. The crosses are connected by black lines to better view the data trends. The red line shows the expected northward velocity component according to the RG-96 model for the conditions considered. In these plots, magnetic local time was used; the UT bin was simply shifted by 6 hours as this is considered to be the difference between the UT and MLT time for the RKN location.

Both the RKN data and model predictions in Figures 8a−8c show similar trends in terms of the velocity transition from positive to negative values around 0600 MLT and reverse transition from negative to positive values around 1800 MLT, as expected for a 2-cell pattern. The model expects maximum positive (negative) velocities during pre-midnight (pre-noon) hours (Figures 8b−8d) and the maxima are to be shifted towards later hours for θ=270°. The RKN data are in agreement with these expectations. In terms of the velocity magnitude, there are significant differences between the model and the data for some periods. For northward IMF (θ=0°) these are not as strong as for the other IMF orientations, but there is an important difference between the model and RKN data at near noon hours. The model does not expect positive velocities here (reverse convection flows) while they were regularly observed over several hours of UT by the RKN radar. For negative IMF B_z (θ=180°) both the near midnight and near noon observed velocity magnitudes were smaller by a factor of roughly 2. The difference in largest/smallest velocities during midnight/noon hours are not strong for positive B_y dominated IMF (θ=90°), but still the observed velocities were smaller. For the IMF negative B_y configuration (θ=270°), the significant difference occurred during near noon hours.

Although the data presented in Figure 8 point at noticeable differences between the model and RKN measurements, our analysis showed that the disagreements are getting smaller at larger radar ranges, i.e. at larger magnetic

latitudes, and at stronger IMF magnitudes. In terms of season, analysis showed that the agreement is getting worse toward the summer.

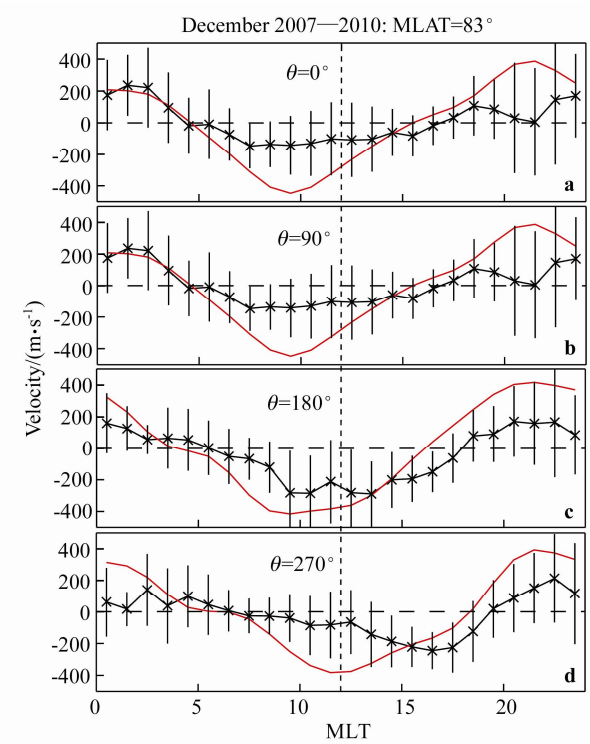

Figure 8 Hourly medians of the RKN velocity (crosses) for beams 6–8, range gates 24–26 versus magnetic local time under various IMF clock angle sectors θ of the Ruohoniemi and Greenwald–1996 model. Vertical bars indicate the standard deviation of the velocity within each bin. The model velocity values (meridional component) are shown by red line. All RKN radar data were obtained for $0 \leqslant B_t \leqslant 4nT$($B_t = \sqrt{B_z^2 + B_y^2}$, where B_z and B_y are the IMF components) as given by the OMNI data set.

4 Discussion

Data presented on typical RKN velocities for observations roughly along the magnetic meridian are consistent with expectations from the body of knowledge on plasma circulation in the polar cap. The data can be explained by assuming that most of the time the plasma circulation pattern consists of two cells with anti-sunward (regular) flow through the central polar cap. On average, the noon "throat" of the flow, an area where the plasma enters the polar cap on the dayside, was shifted toward morning hours, as expected[14]. Under sufficiently strong IMF B_z conditions, the reverse (sunward) flows were seen, but only very close to the magnetic noon.

Although the data are consistent with general understanding, several interesting details emerged. One is with respect to reverse plasma flows. It is clear that such flows occur under positive IMF B_z on the dayside and they do not extend to the nightside as almost no negative velocities were detected during near midnight hours while positive velocities often occurred near noon (Figures 2a, 6d). We examined RKN data for larger latitudes and found that the amount of midnight negative velocities increases with latitude but at MLATs> 85° the amount of available measurements drops drastically so that no clear conclusion can be made. In this respect, it would be interesting to investigate the effect with McMurdo radar data because this radar detects echoes at larger latitudes, all the way to the magnetic pole.

An important conclusion with respect to the reverse flows is their alignment with the magnetic meridian, Figure 4; no reverse flows were seen in beams 0−2 and 13−15 that are much more off the magnetic meridian (for beam orientation, Figure 1). Such flows occur in a very short time period of about two hours around magnetic noon, and they seem to be stronger in beams 9−11 whose orientations are very close of the magnetic meridian. Typical magnitudes of the reverse flows were rather low, <100 m·s^{-1}. We note that this is an apparent effect as we presented in Figure 4 the median velocity for each hour of observations. Individual velocity of a reverse flow can be as large as 800 m·s^{-1}, see for example Figure 6b.

Long-term data on the RKN velocity for observations at MLAT=83° (Figure 5) showed that reverse plasma flows are consistently faster during spring equinoxes. The reverse flows were also seen during the summer and during fall equinox at larger MLATs. The reason for lower velocities of winter reversed flows is not clear. One of possible explanations is more favorable conditions for the lobe reconnection (under positive IMF B_z) in the summer hemisphere as discussed, for example, by Crooker and Rich[15].

The second interesting feature of the data presented is the difference in the MLT times for a change in the velocity polarity for observations during dawn hours, Figure 4b. According to Figure 4b, the polarity changes first at far ranges (large MLATs) and later at shorter ranges (smaller MLTs). This feature is seen in other beams/directions of observations as well (Figure 4). This is an indication that the polar cap flow is not uniformly antisunward at MLAT= 83°; it seems to be crescent-like even at these latitudes. Ruohoniemi and Greenwald[16] showed various degrees of "curving" for the crescent part of the convection pattern, depending on the IMF conditions. Our data seem to be consistent with their B_y^+ dominating pattern (their Figure 5).

Our results with respect to the regular antisunward flows are consistent with expectations. The magnitudes of the near noon flows were somewhat larger on the nightside as compared to the dayside (Figure 2a, and compare the distributions of negative velocities in Figure 6a with the distributions of positive velocities in Figure 6b). We note that this noon-midnight difference varies with range and season. We found that at shorter ranges and especially during winter, the around noon velocity magnitudes are usually larger than the midnight velocities. In the midnight sector, the most east- (west-) oriented beams measured largest (smallest) velocities. This difference is surprising as beams 0−2 and 13−15 are almost symmetrically oriented with respect to the magnetic L-shells and one would expect very

comparable velocities if the 2-cell convection pattern dominates. In the noon sector, largest velocity magnitudes were also detected in the most east-oriented beams 13−15.

We showed (Figure 7) that the meridional flows are faster for larger IMF B_z and IEF magnitudes. This is consistent with earlier limited analysis by Fiori et al.[3] who showed that the RKN velocity for near noon observations along the magnetic meridian increases linearly with the PCN magnetic index. The PCN index is a good proxy for IEF[17]. More recently, Bristow et al.[18] showed that McMurdo velocity of the flow along the noon-midnight meridian increases linearly with the IMF B_z and IEF magnitude with some evidence for the velocity saturation at large magnitudes. The typical McMurdo velocity values were <400 m·s^{-1} with maximum observed velocities of ~600 m·s^{-1}. It should be noted that Bristow et al.[18] presented the component of the flow, the total velocities were larger. The RKN data presented in this study are fully consistent with the above notion of larger velocity at stronger external drivers. Moreover, the slopes of the linear fit lines were larger than the ones for the McMurdo data[18]. We comment that no clear saturation effect was seen in our data; however, few points were available for IEF>3 mV·m^{-1} for which the effect is highly expected[3].

A comparison performed between the RKN velocities and expectations of the RG-96 statistical model gave mixed results. Trends in the data for various orientations of the IMF were similar but the velocity magnitudes were often significantly smaller. In many occasions the model velocity magnitude was larger than the median velocity magnitude plus the standard deviation of the median velocity in hourly bins. One of the reasons for larger model velocities could be the fact that the RG-96 model is based on the Goose Bay data collected for periods of both low and strong solar activity. In this study we demonstrated that with intensification of external drivers (controlled by the Sun) the RKN HF velocities tend to be larger. As additional testing, we processed Saskatoon radar data for March 2010 and found that hourly velocity medians values at latitudes >80° are consistent with the RKN data.

Another factor to consider is the occurrence of low-velocity RKN echoes. These might affect the median velocities in a significant way. For example, this was the case for December 2010 when few reverse flow velocities were observed but the velocity medians were still around zero (the raw data were not presented here). As mentioned earlier, the low-velocity data could be a mixed ionospheric-ground scatter echoes. The more frequent occurrence of such echoes during daytime with generally better propagation conditions and preferential occurrence of ground scatter[12] favor this explanation, but more definite analysis needs to be done.

5 Conclusions

The results of this study can be summarized as follows.

(1) For meridionally-oriented radar beams the statistically typical RKN velocity shows clear magnetic local time variation with maximum positive (negative) velocity occurring during pre-midnight (pre-noon) hours. Maximum velocity values are between 400−500 m·s^{-1}, independent on the season. The MLT velocity variation is consistent with the 2-cell convection pattern with the exception that close to the magnetic noon, within plus-minus one hour, and at MLATs>82°−83° the reverse (towards the Sun) plasma flows occur. These reverse flows occur for the periods of positive IMF B_z component. Over 5 years of observations, the reverse flows were found to be strongest during equinoctial/summer time.

(2) The velocity magnitude increases almost linearly with the IMF B_z and interplanetary electric field. The data did not show the velocity saturation effect but neither IMF nor IEF reached the values for which the saturation effect has been seen in data from other instruments.

(3) The RKN velocity magnitude distribution is often affected by the presence of low-velocity echoes whose velocity magnitude is below 50 m·s^{-1}. Such echoes often dominate during daytime and at larger radar ranges. These echoes were excluded from consideration in the current study.

(4) The MLT variation of the typical RKN velocity (for relatively small IMF B_t and winter conditions) are consistent with expectations of the statistical model of plasma circulation at high latitudes by Ruohoniemi and Greenwald–1996 but the velocity magnitudes are somewhat smaller than expected.

Acknowledgements The PolarDARN HF radars are operated by the University of Saskatchewan radar group with funding from the Canadian Space Agency and National Science and Engineering Research Council (NSERC). This work was supported by NSERC Discovery grant to AVK and the University of Saskatchewan graduate stipend to MG. We thank NASA Goddard Space Flight Center for making the IMF and solar wind data available through the OMNIWeb site.

References

1 Ruohoniemi J M, Greenwald R A. Statistical patterns of high-latitude convection obtained from Goose Bay HF radar observations. J Geophys Res, 1996, 101(A10): 21743-21763.

2 Liu H. Study of the high-latitude ionosphere with the Rankin Inlet PolarDARN radar. Saskatchewas: University of Saskatchewan, 2010.

3 Fiori R A D, Koustov A V, Boteler D, et al. PCN magnetic index and average convection velocity in the polar cap inferred from SuperDARN radar measurements. J Geophys Res, 2009, 114, A07225, doi: 10.1029/2008JA013964.

4 Koustov A V, Sofko G J, André D, et al. Seasonal variation of HF radar F region echo occurrence in the midnight sector. J Geophys Res, 2004, 109, A06305, doi: 10.1029/2003JA010337.

5 Tsunoda R T. High-latitude F region irregularities: A review and synthesis. Rev Geophys, 1988, 26: 719-760.

6 Chisham G, Pinnock M. Assessing the contamination of SuperDARN global convection maps by non-*F*-region backscatter. Ann Geophys, 2002, 20(1): 13-28.

7 Koustov A V, St. Maurice J P, Sofko G J, et al. Three-way validation of

the Rankin Inlet PolarDARN radar velocity measurements. Radio Sci, 2009, 44, RS4003, doi: 10.1029/2008RS004045.

8 Mori D, Koustov A V, Jayachandran P T, et al. Resolute Bay CADI ionosonde drifts, PolarDARN HF velocities, and cross polar cap potential. Radio Sci, 2012, 47, RS3003, doi:10.1029/2011RS004947.

9 Fukumoto M, Nishitani N, Ogawa T, et al. Statistical analysis of echo power, Doppler velocity and spectral width obtained with the Syowa South HF radar. Adv Polar Upper Atmos Res, 1999, (13): 37-47.

10 Nishitani N, Lester M, Milan S E, et al. Unusual ionospheric echoes with high velocity and very low spectral width observed by the SuperDARN radars in the polar cap during high geomagnetic activity. J Geophys Res, 2002, 109, A02311, doi: 10.1029/2003JA010048.

11 Milan S E, Yeoman T K, Lester M, et al. Initial backscatter occurrence statistics from the CUTLASS HF radars. Ann Geophys, 1997, 15(6): 703-718.

12 Ponomarenko P V, St. Maurice J P, Hussey G C, et al. HF ground scatter from the polar cap: Ionospheric propagation and ground surface effects. J Geophys Res, 2010, 115, A10310, doi: 10.1029/2010JA015828.

13 Pettigrew E D, Shepherd S G, Ruohoniemi J M. Climatological patterns of high-latitude convection in the northern and southern hemispheres: Dipole tilt dependencies and interhemispheric comparisons. J Geophys Res, 2010, 115, A07305, doi: 10.1029/JA014956.

14 Kustov A V, Lyatsky W B, Sofko G J, et al. Field-aligned currents in the polar cap at small IMF B_z and B_y inferred from SuperDARN radar observations. J Geophys Res, 2000, 105(A1): 205-214.

15 Crooker N U, Rich F J. Lobe cell convection as a summer phenomenon. J Geophys Res, 1993, 98(A8): 13403-13407, doi: 10.1029/93JA01037.

16 Ruohoniemi J M, Greenwald R A. Dependencies of high-latitude plasma convection: Consideration of interplanetary magnetic field, seasonal, and universal time factors in statistical patterns. J Geophys Res, 2005, 110, A09204, doi: 10.1029/2004JA010815.

17 Troshichev O, Janzhura A, Stauning P. Unified PCN and PCS indices: Method of calculation, physical sense, and dependence on the IMF azimuthal and northward components. J Geophys Res, 2006, 111, A05208, doi: 10.1029/2005JA011402.

18 Bristow W A, Spaleta J, Parris R T. First observations of ionospheric irregularities and flows over the south geomagnetic pole from the Super Dual Auroral Radar Network (SuperDARN) HF radar at McMurdo Station, Antarctica. J Geophys Res, 2011, 116, A12325, doi: 10.1029/2011JA016834.